frontiers in Earth Science

ORIGINAL RESEARCH
published: 22 April 2021
doi: 10.3389/feart.2021.661581

The Effect of Diagenetic Evolution on Shale Gas Exploration and Development of the Longmaxi Formation Shale, Sichuan Basin, China

Jia Wang[1,2,3], Xianfeng Tan[3]*, Jingchun Tian[1], Long Luo[3], Xuanbo Gao[3], Chao Luo[4], Chunlin Zeng[5], Lei Zhang[3] and Weiwei Xue[6]*

[1] Institute of Sedimentary Geology, Chengdu University of Technology, Chengdu, China, [2] Shandong Provincial Key Laboratory of Depositional Mineralization & Sedimentary Mineral, Shandong University of Science and Technology, Qingdao, China, [3] Chongqing Key Laboratory of Complex Oil and Gas Exploration and Development, Chongqing University of Science and Technology, Chongqing, China, [4] Exploration and Development Research Institute of Southwest Oil and Gas Field Company, PetroChina, Chengdu, China, [5] Chongqing Institute of Geology and Mineral Resources, Chongqing, China, [6] School of Earth Science and Engineering, Nanjing University, Nanjing, China

OPEN ACCESS

Edited by:
Dawei Lv,
Shandong University of Science and Technology, China

Reviewed by:
Ruyue Wang,
SINOPEC Petroleum Exploration and Production Research Institute, China
Kaikai Li,
China University of Geosciences, China

***Correspondence:**
Jia Wang
wangjia@cqust.edu.cn.com
Xianfeng Tan
xianfengtan8299@163.com

Specialty section:
This article was submitted to Sedimentology, Stratigraphy and Diagenesis, a section of the journal Frontiers in Earth Science

Received: *02 February 2021*
Accepted: *26 February 2021*
Published: *22 April 2021*

Citation:
Wang J, Tan X, Tian J, Luo L, Gao X, Luo C, Zeng C, Zhang L and Xue W (2021) The Effect of Diagenetic Evolution on Shale Gas Exploration and Development of the Longmaxi Formation Shale, Sichuan Basin, China. Front. Earth Sci. 9:661581. doi: 10.3389/feart.2021.661581

Diagenetic evolution is an important controlling factor of shale gas reservoirs. In this study, based on field outcrop and drilling core data, analytical techniques including X-ray diffraction (XRD), field emission scanning electron microscope combined with a focused ion beam (FIB-FESEM), and energy-dispersive spectroscopy (EDS) analyses were performed to determine the diagenetic evolution of the Longmaxi Formation shale and reveal the effect of diagenetic evolution on the shale gas exploration and development in the Sichuan Basin, Southwest China. The eodiagenesis phase was subdivided into two evolution stages, and the mesodiagenesis phase was subdivided into three evolution stages in the basin margin and center. Absorbed capacity and artificial fracturing effect of the Longmaxi Formation shale gas were related to mineral composition, which was influenced by sedimentary characteristics and diagenetic evolution. The diagenetic system in the basin margin was more open than that in the basin center due to a different burial history. The more open diagenetic system, with more micro-fractures and soluble constitute (e.g., feldspar), was in favor for the formation and preservation of secondary dissolved pores and organic pores in the basin margin. The relatively closed diagenetic system with stronger compaction resulted in deformation of pore space in the central basin.

Keywords: shale, diagenetic evolution, structural evolution, organic matter, Longmaxi Formation, Sichuan Basin

INTRODUCTION

Shale gas, which is a kind of "self-generation and self-accumulation" gas reservoir, is a major unconventional hydrocarbon resource (Jarvie et al., 2007; Zou et al., 2016). Reservoir quality is key to shale gas exploration and development (Wang et al., 2018; Wang R. Y. et al., 2019; Wang et al., 2020a; Jia et al., 2019; Wang X. et al., 2019), which is mainly influenced by sedimentary

characteristics (Lv et al., 2020), structural history, and diagenetic evolution (Bjørlykke, 2014). In fact, sedimentary characteristics and structural history generally influenced reservoir quality by controlling diagenetic evolution (Dickinson, 1993; Bjørlykke and Jahren, 2012). However, previous studies have mainly focused on the diagenetic systems of conventional reservoirs (Bjørlykke and Jahren, 2012; Luo et al., 2019) but rarely report the diagenetic system of argillaceous (Lv et al., 2019) and other unconventional rocks (Day-Stirrat et al., 2010).

The study of diagenetic systems originated in the 1970s and 1980s and mainly focused on the diagenetic relationship between diagenesis and the evolution products of organic matter in deep clastic rock (Curtis, 1978; Boles and Franks, 1979). Subsequently, models of organic–inorganic interactions (Surdam et al., 1984; Burtner and Warner, 1986; Surdam, 1989; Buhman, 1992; Bjørlykke, 1993; Li and Li, 1994; Schoenherr et al., 2007), regional diagenesis (Seiver, 1979; Li and Li, 1994), and basin geological systems (Allen and Allen, 1990; Dickinson, 1993; Li, 1995; Dickinson et al., 1997) were proposed and promoted. In the early 2000s, scholars began to study the diagenesis process in terms of basin dynamics and focused their attention on the relationships between microscopic diagenetic characteristics and basin evolution or thermal fluid activity (Li et al., 2003; Archer et al., 2004; Bjørlykke and Jahren, 2012; Meng et al., 2012; Lv et al., 2015; Lai et al., 2016; Yuan et al., 2017, 2019). Consequently, the diagenetic system became a multi-dimensional research field (Li et al., 2003; Archer et al., 2004; Bjørlykke, 2014; Yuan et al., 2015, 2017; Lv et al., 2015; Lai et al., 2015, 2017, 2018; Luo et al., 2019).

During the research processes of exploration and development of shale gas (Schmoker, 1993; Curtis, 2002; Law and Curtis, 2002; Jarvie et al., 2007; Zhang et al., 2008; Zou et al., 2016), many researchers found that argillaceous rocks were influenced by tectonic evolution, geochemistry of basinal fluids, and several other factors concerning the transformation of minerals and organic hydrocarbon generation during the burial process (Robert et al., 2009; Milliken et al., 2012; Wang et al., 2015, 2020b; Kong et al., 2015; Dong et al., 2015; Luan et al., 2016; Zhao et al., 2016). The physical characteristics of shale and the enrichment ability of shale gas are understood to be largely restricted by the aforementioned factors (Jarvie et al., 2007; Loucks et al., 2009). This study aims to recover the whole diagenetic evolution process of argillaceous rocks and to reveal the effects of diagenetic evolution on shale gas exploration and development by using the Longmaxi Formation, Southwestern China, as a case study.

GEOLOGICAL SETTING

The Sichuan Basin is a petroliferous basin in Southwestern China, which is bounded by the fault zone of Longmen Mountain to the west, the fault zone of the Micang and Daba mountains to the north, and the Hunan-Guizhou-Hubei fold belt to the southeast (He et al., 2000; Zhao et al., 2003; Li, 2013). The geomorphic features are characterized by the north to northeast trending mountain range, which alternates with the northeast trend of the small intermontane basin and surface structures (**Figure 1A**). The Lower Silurian Longmaxi Formation in the study area

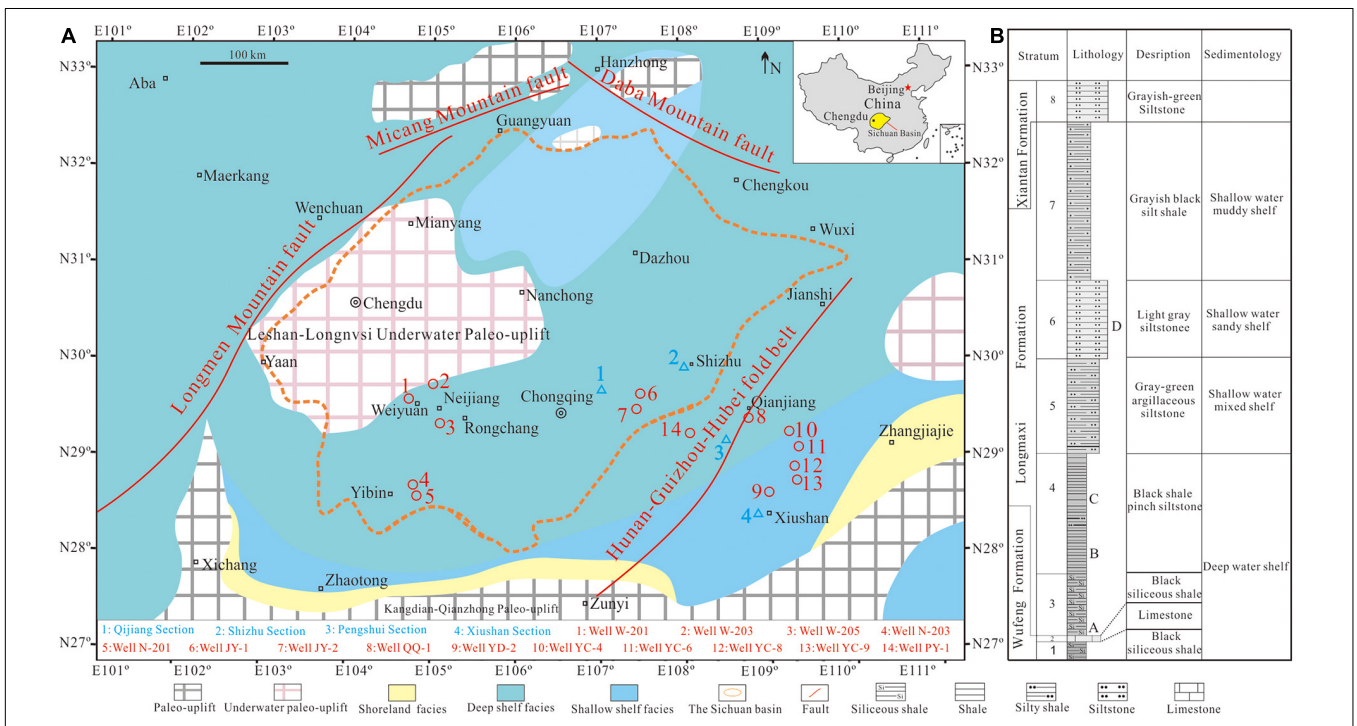

FIGURE 1 | A map **(A)** showing sedimentary characteristics and sampling locations of the Sichuan Basin (the inset map shows the basin location within China) (modified after Mou et al. (2011)). **(B)** The stratigraphic characteristics of the Longmaxi Formation in Xiushan section.

has a thickness of 60–120 m and was mainly deposited in a low-energy, anoxic marine shelf environment. The sedimentary paleogeography of the Longmaxi Formation shale was controlled by many uplifts such as the Kangdian-Qianzhong paleo-uplift and the Leshan-Longnvsi underwater paleo-uplift (**Figure 1A**; Liang et al., 2008; Wang et al., 2011; Wang J. et al., 2014). The lower part of the Longmaxi Formation consists of black siliceous shale, which was deposited in deep-water shelf facies (Mou et al., 2011). The middle part of the formation consists of black siliceous shale of deep-water shelf facies and black carbonaceous shale of shallow-water mixed shelf facies, whereas the upper part comprises silty mudstone or argillaceous siltstone of argillaceous shelf facies that deposited in a shallow, sandy continental shelf (Mou et al., 2011; **Figure 1B**).

SAMPLES AND METHODS

The Longmaxi Formation shale of five wells was analyzed in the central Sichuan Basin (**Figure 1A**). The Longmaxi Formation shale of nine wells and four field sections were studied in the basin margin (**Figure 1A**). The related data of seven wells (W-201, W-203, W-205, N-201, N203, JY-1, and JY-2) were collected from a previous research (**Figure 1A** and **Table 1**). In addition, 177 drilling cores (seven wells) and 111 field outcrop (four sections) samples of the Longmaxi Formation shale in the Sichuan Basin were collected in this study (**Figure 1A**). Large fragments from each sample were firstly removed for field emission scanning electron microscope combined with a focused ion beam (FIB-FESEM) analysis. All microscopic analyses were conducted at the State Key Laboratory of Oil and Gas Reservoir Geology and Exploitation, Chengdu University of Technology, China. A Quanta FEG 250 environmental FESEM was used with image magnifications of between 10 and 500,000. The samples were analyzed using a relatively low beam energy in a high-pressure (∼60 Pa) vacuum chamber environment, and the energy-dispersive spectroscopy (EDS) was performed on some important observation points of samples using the Oxford INCA X-Max20. Meanwhile, a gallium ion beam was then used to prepare planar cross sections for FESEM observation; four cross sections were prepared on shale samples; each planar cross-section prepared by FIB milling was typically 100 $\mu m^2 \times 100\ \mu m^2$ and 30–50 FESEM images. Finally, the three-dimensional imaging analysis of pores was realized by FIB-FESEM.

Some small samples were selected and dried at a low temperature before being ground into a 200 mesh. To remove carbonate rock before testing, 10% hydrochloric acid was subsequently added to each sample in a centrifuge tube and glass beaker. X-ray powder diffraction for all samples were obtained using a Bruker D8 ADVANCE at the State Key

TABLE 1 | Organic geochemial parameters of the Longmaxi Formation shale in the Sichuan Basin.

Region	Well/section	Number of samples	Rb (average, %)	Ro (average, %)	T_{max} (average,°C)	TOC (average, %)
Basin margin (Southeast Sichuan Basin)	QQ-1 well	19	3.50	2.56	489.70	2.64
	YQ-1 well	10	3.71	2.69	–	2.72
	PY-1 well	17	3.53	2.58	–	2.83
	Shizhu section	21	3.05	2.28	502.30	2.51
	Xiushan section	9	3.76	2.72	513.50	1.98
Basin center (Southwest Sichuan Basin)	W-201 well	43	2.77	2.11	–	1.89
	W-203 well	37	3.87	2.72	–	2.62

Rb, bitumen reflectance; Ro, vitrinite reflectance, according to the formula Ro = 0.618 × Rb + 0.4 (Jacob, 1985); T_{max} maximum pyrolysis peak temperature; TOC, total organic carbon. En dash indicates that the measurement is not available. The data of well W-201 and well W-203 are referenced from Wu (2018).

TABLE 2 | Mineral compositions of the organic-rich shale in the Sichuan Basin (XRD).

Location	Well/section (number of samples)	Quartz content (min–max/average, %)	Feldspar content (min–max/average, %)	Carbonate content (min–max/average, %)	Pyrite content (min–max/average, %)	Clay content (min–max/average, %)	Brittle content (min–max/average, %)
Basin margin (Southeast Sichuan Basin)	JY-1 well	18.4–70.6/44.4	3.2–15.0/8.3	0.0–31.5/9.7	0.0–4.8/0.5	16.6–62.8/40.9	37.2–83.4/59.1
	QQ-1 well (43)	32.0–70.0/45.9	3.0–20.0/12.6	0.0–12.0/6.4	0.0–8.0/2.3	16.0–58.0/35.2	40.0–81.0/64.9
	YD-2 well (13)	30.8–70.0/41.6	4.6–25.0/14.8	2.1–19.8/10.0	1.5–6.5/3.1	16.6–42.2/29.6	53.7–79.2/66.4
	YC-4 well (35)	27.4–49.2/35.8	6.9–19.3/12.3	2.8–24.6/8.9	2.2–5.3/4.1	17.0–50.9/38.2	49.2–77.9/61.1
	YC-6 well (23)	27.9–56.8/40.0	4.7–28.1/16.8	2.3–21.6/11.1	0.0–7.3/2.6	3.6–50.1/27.8	40.9–93.1/67.9
	YC-8 well (25)	25.7–52.2/40.8	1.7–28.7/16.9	0.2–23.5/9.4	0.0–7.0/2.5	7.1–58.2/29.3	39.5–90.7/67.1
	YC-9 well (38)	9.3–93.1/52.3	0.0–71.1/11.1	0.0–84.0/9.2	0.3–18.7/8.1	3.8–34.6/17.2	51.5–95.9/72.6
	Sections (111)	25.7–70.0/41.9	1.7–28.7/15.7	0.0–23.5/9.1	0.0–8.0/2.5	3.6.0–58.2/29.6	39.5–93.1/66.7
Basin center (Southwest Sichuan Basin)		25.3–65.3/50.0	0.0–9.1/3.4	7.9–19.9/13.3	0.0–2.2/0.6	26.5–53.4/29.7	43.4–73.5/66.7

The data of the Southeast Sichuan Basin are consist of sections of Shizhu, Pengshui, Xiushan, and Qijiang. The data of the Southwest Sichuan Basin are referenced from Wu (2018). The data of JY-1 well are referenced from Guo et al. (2014).

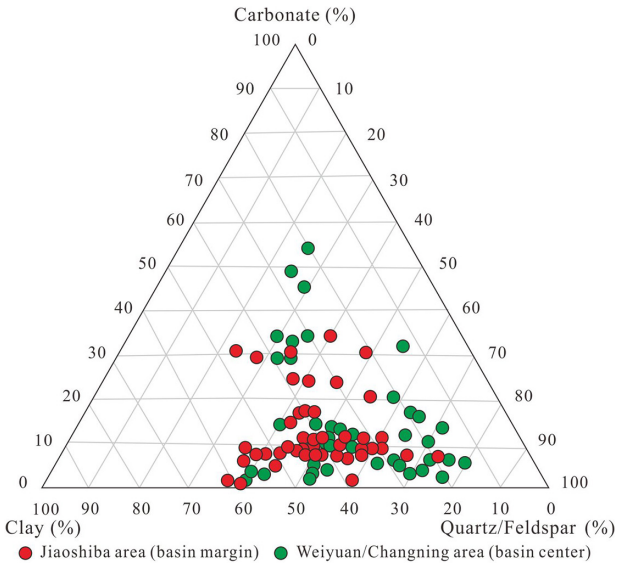

FIGURE 2 | A ternary diagram showing mineral compositions of shale samples in the Sichuan Basin (the data of Jiaoshiba area was referenced from Guo et al. (2014)).

Laboratory of Oil and Gas Reservoir Geology and Exploitation (Chengdu University of Technology, China) under 25°C and 50% humidity. Seventy-six samples (46 samples from wells and 30 samples from sections) were analyzed for total organic carbon (TOC) and bitumen reflectance (Rb), respectively, using a LECO CS230 carbon and a Leica MPV-III microphotometer under oil immersion, and the Rock-Eval parameters including volatile hydrocarbon content (S_1), remaining hydrocarbon generative potential (S_2), and temperature at maximum generation (T_{max}) values were determined using ROCK-EVAL 6 (RE6) at the Sichuan Coalfield Geology Bureau.

Density, porosity, and permeability data test of well YQ1 (10 samples) and QQ1 (43 samples) were analyzed in the Chongqing Key Laboratory of Complex Oil and Gas Exploration and Development using an automated permeameter-porosimeter (AP-608) and V-Sorb 2800TP. In addition, the diagenesis of the Longmaxi Formation black shale was determined by means of field outcrop and core observations.

RESULTS

Organic Geochemical Characteristics

Generally, TOC average values of the Longmaxi Formation shale are generally more than 2.0% (average, 1.89–2.83%) (**Table 1**). Typically, TOC values of shale in the lower part of the Longmaxi Formation are more than 3.0% (Wang et al., 2020b). The mean values of vitrinite reflectance (Ro) of each outcrop profile and well, which were calculated by bitumen reflectance (Rb) and Jacob's calculation formula ($Ro = 0.618 \times Rb + 0.4$), are generally greater than 2.5% (2.11–2.72%) in the basin margin and center (**Table 1**). T_{max} average values are greater than 480°C (489.70–513.50°C) in basin margin (**Table 1**). There is no obvious difference in TOC values between basin margin and center.

Mineralogy and Diagenesis Characteristics

Mineralogy

The Longmaxi Formation in the Sichuan Basin mainly consists of interbedded shale and argillaceous siltstone with unequal thicknesses. The average quartz contents of the shale vary from 35.8 to 52.3% in the Sichuan Basin margin, which were less than those (average, 50%) in the southwestern Sichuan Basin (basin center) (**Table 2** and **Figure 2**). The average carbonate mineral content of the Longmaxi Formation shale varies from 6.4 to 11.1% in the southeastern Sichuan Basin (basin margin), which were generally less than the average carbonate mineral content (average, 13.3%) in the southwestern Sichuan Basin (basin center) (**Table 2**). The carbonate mineral content of the Longmaxi Formation shale in the central basin (e.g., Weiyuan, Rongchang, and Zhaotong area) is more than 20% (Wang et al., 2020b). On the contrary, the average feldspar contents range from 8.3 to 16.9% in the basin margin and 3.4% in the basin center

TABLE 3 | Clay mineral compositions of the Longmaxi Formation shale in the Sichuan Basin (XRD).

Region	Wells	Number of samples	Clay mineral content (min–max/average, %)				Mixed layer ratio (min–max/average, S%)	
			Illite	Chlorite	Illite–smectite	Chlorite–smectite	Illite–smectite	Chlorite–smectite
Basin margin (Southeast Sichuan Basin)	YC-4	35	10–47/21.6	1–19/9.0	41–82/60.0	1–14/7.4	5–11/6.8	10–15/11.4
	YC-6	23	15–46/25.5	6–16/9.2	40–70/59.5	3–10/6.2	6–11/8.2	9–15/11.8
	YC-8	25	12–29/18.3	5–13/8.7	52–80/67.9	2–11/5.1	5–10/7.1	10–16/11.8
	YC-9	38	11–84/47.7	0–12/0.8	16–75/50.8	0–10/0.7	4–10/6.1	0–11/0.8
	QQ-1	43	40–53/45.8	6–18/10.9	33–49/43.3	0–8/0.5	5–10/8.2	1–14/7.9
	YD-2	13	38–62/52.3	2–10/6.8	32–60/40.9	0–8/0.5	8–10/9.1	1–10/5.6
Basin center (Southwest Sichuan Basin)	W-201	65	3–95/50.8	3–93/25.6	5–94/23.3	–	–	–
	W-205	17	22–70/45.8	0–10/10.6	0–57/33.0	-	–	–

The data of well W-201 and well W-205 are referenced from Wu (2018). En dash indicates that the measurement is not available.

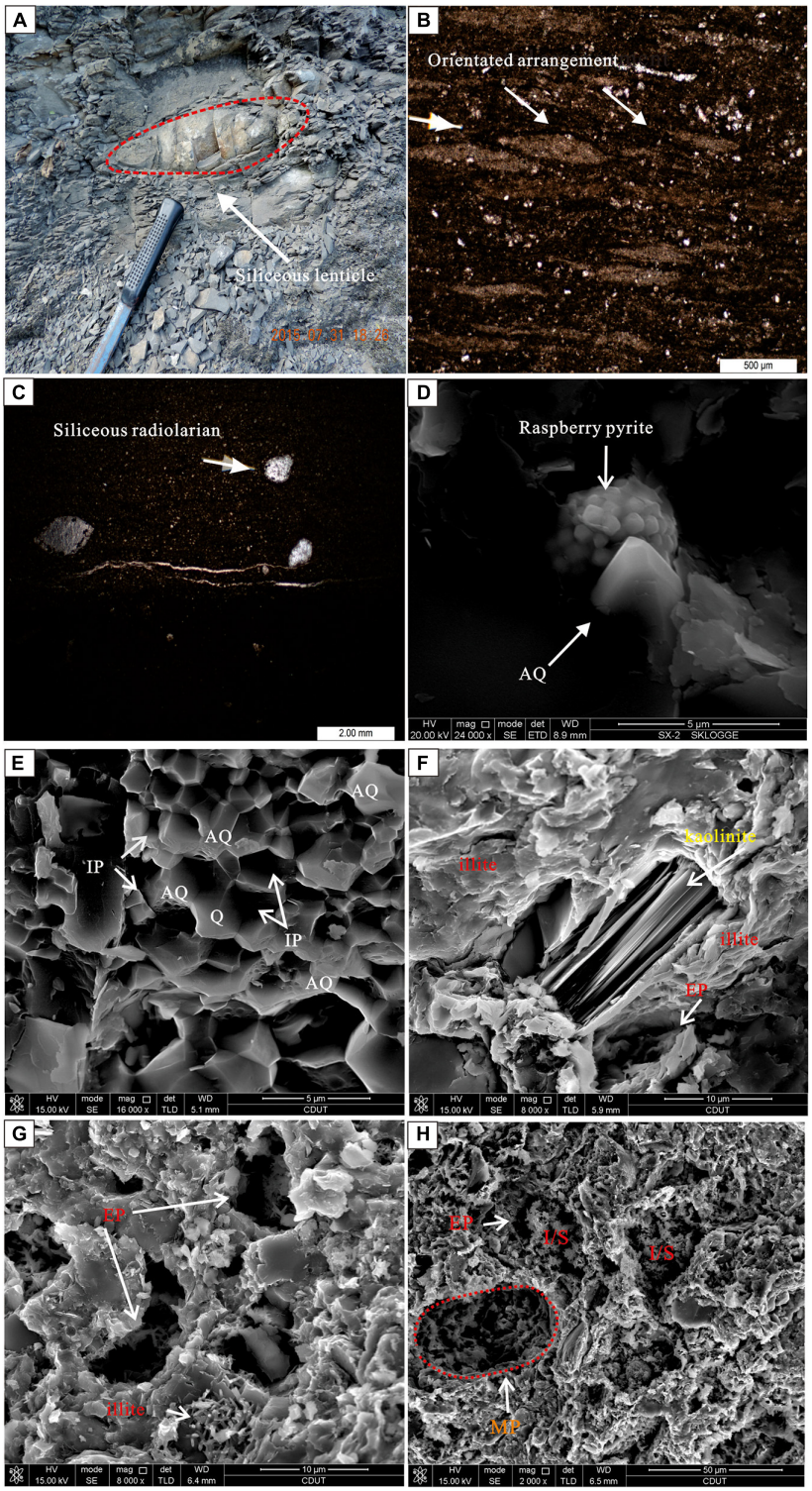

FIGURE 3 | Types and characteristics of pore spaces of the Longmaxi Formation shale in the Sichuan Basin [micrographs of thin sections and scanning electron microscope (SEM)]. **(A)** A photograph of the Longmaxi Formation Shale in the Xiushan field outcrop, showing the siliceous lenticle. **(B)** Micrographs of thin sections (MTS) showing the orientated arrangement of minerals, the Xiushan section, layer 3. **(C)** Micrographs of thin sections (MTS) showing the siliceous radiolarian, the Shizhu section, layer 4. **(D)** An SEM image showing strawberry pyrite and authigenic quartz (AQ), the Pengshui section, layer 2. **(E)** An SEM image showing inter-crystalline pores (IP) of authigenic quartz, the Shizhu section, layer 2. **(F)** An SEM image showing intergranular pores (EP) of clay minerals, the Xiushan section, layer 5. **(G)** An SEM image showing intergranular pores (EP) of illite, the Qijiang section, layer 6. **(H)** An SEM image showing intergranular pores (EP) and molded pores (MP) of illite–smectite mixed minerals, the Qijiang section, layer 5.

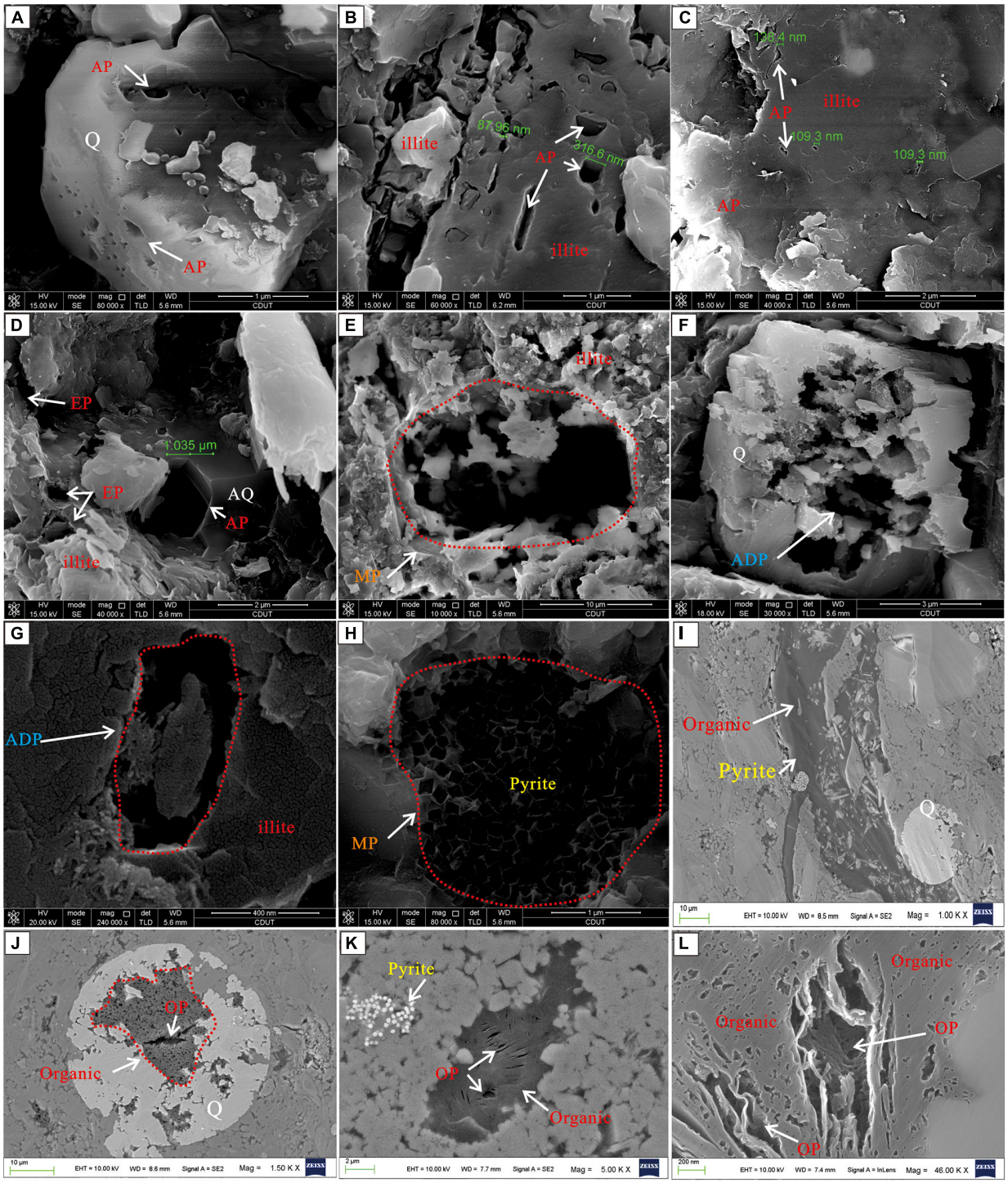

FIGURE 4 | Types and characteristics of pore spaces of the Longmaxi Formation shale in the Sichuan Basin [scanning electron microscope (SEM) and field emission scanning electron microscope (FESEM)]. **(A)** An SEM image showing intragranular pores (AP) of authigenic quartz (AQ), the Shizhu section, layer 4. **(B)** An SEM image showing intragranular pores (AP) of illite, the Xiushan section, layer 5. **(C)** An SEM image showing intragranular pores (AP) of illite, the Pengshui section, layer 4. **(D)** An SEM image showing intergranular pores (EP) of illite and intragranular pores (AP) of quartz, the Pengshui section, layer 7. **(E)** An SEM image showing intragranular dissolved pores (ADP) of quartz, the Xiushan section, layer 3. **(F)** Intragranular dissolved pores (ADP) of quartz, the Shizhu section, layer 4. **(G)** An SEM image showing intragranular dissolved pores (ADP), the Qijiang section, layer 7. **(H)** An SEM image showing molded pores (MP) of strawberry pyrite, the Pengshui section, layer 5. **(I)** An FESEM image showing organic matter and pyrite, well JY-2, 2,459.34 m. **(J)** An FESEM image showing organic micropore (OP), well JY-2, 2,459.36 m. **(K)** An FESEM image showing organic micropores (OPs) and pyrite, well W-201, 2,678.61 m. **(L)** An FESEM image showing organic micropores (OPs), well N-203, 2,325.64 m.

(**Table 2**). The average content of clay mineral in the basin margin (17.2–40.9%) is more than that in the basin center (average, 29.7%) (**Table 2**). The average contents of brittle mineral in the basin margin (59.1%–72.6%) are slightly more than those in the basin center (66.7%) (**Table 2** and **Figure 2**).

Diagenetic Characteristics

Clay mineral transformations

Clay minerals in the Longmaxi Formation shale mainly comprise illite, mixed illite–smectite, mixed chlorite–smectite, and chlorite (**Table 3**). The average illite content ranges from 18.3 to 52.3% in the basin margin, which is generally less (average, 45.8–50.8%) than that in the basin center (**Table 3**). The average chlorite content of the basin margin (0.8%–10.9%) is less than that in the basin center (10.6–25.6%) (**Table 3**). In contrast, the average mixed illite–smectite content in the basin margin (40.9–67.9%) is more than that in the basin center (average, 23.3–33.0%) (**Table 3**). The content of mixed chlorite–smectite in the basin margin ranges from 0.5 to 7.4% (**Table 3**). The smectite content of mixed illite–smectite ranges from 6.1 to 9.1 % in the basin margin (**Table 3**). The smectite contents within mixed chlorite–smectite vary from 0.8 to 11.8 % in the basin margin (**Table 3**).

Compaction

At outcrop, the shale samples are very tight and hard (**Figure 3A**). Clay minerals, organic matter, and mica in the shale were clearly aligned under the microscope (**Figure 3B**).

Silicification

The tight siliceous lenticle, whose diameters range from 0.1 to 0.5 m, was observed in the shale of the field outcrop (**Figure 3A**). Siliceous radiolarian shaped like ellipticity occurred as the result of biogenetic silicification (**Figure 3C**). Pore-filling authigenic quartz generally were observed under a scanning electron microscope (SEM) (**Figures 3D,E**).

Dissolution

The dissolution of the Longmaxi Formation shale generally occurred in soluble constituents, such as calcite, feldspar, and quartz, or at the edges of clay minerals and formed secondary pores or even molded pores (**Figures 4E,G,H**). Besides, some quartz grains were also dissolved by alkaline fluids (**Figure 4F**).

Pore Characteristics and Physical Property of the Reservoir

Pore spaces mainly consisted of inter-crystalline pores (**Figure 3E**), intergranular pores (**Figure 3F–H**), intragranular primary pores (**Figures 4A–D**), intragranular dissolved pores (**Figures 4E–G**), molded pores (**Figures 3H**, **4H**), organic pores (**Figures 4I–L**), and micro-fractures (**Figure 3F**). The intergranular pores, whose diameters range from 1 to 10 μm, were mainly developed in brittle minerals such as quartz and feldspar. In contrast, the intragranular pores were relatively less than intergranular pores in the brittle minerals. Dissolved pore spaces were widely developed on the surface of calcite and feldspar (diameters 0.1–10 μm). The diameters of organic matter pores range from 50 to 800 nm, which were distinguishable under FESEM (**Figures 4I–L**). Organic pores were extensively prevalent

TABLE 4 | Density, porosity, permeability, and specific surface area of the Longmaxi Formation shale in different wells.

Sample number	Well depth (m)	Density (g/cm^3)	Porosity (%)	Permeability ($\times 10^{-3}\mu m^2$)	Specific surface (m^2/g)
YQI-01	1,136.91	2.69	1.64	0.0001	1.63
YQI-02	1,141.20	2.69	1.58	0.0005	1.43
YQI-03	1,145.55	2.66	1.78	0.0001	1.73
YQI-04	1,147.62	2.66	1.42	0.0001	4.06
YQI-05	1,152.60	2.65	1.71	< 0.0001	1.92
YQI-06	1,155.13	2.61	1.45	0.0286	5.17
YQI-07	1,159.17	2.68	1.78	0.0001	2.01
YQI-08	1,163.11	2.64	1.58	0.0020	2.45
YQI-09	1,164.55	2.67	1.46	0.0001	2.10
YQI-10	1,166.00	2.64	1.23	0.0097	1.22
QQ1-01	707.20	2.64	1.70	0.0312	-
QQ1-02	709.30	2.65	2.00	0.0071	-
QQ1-03	711.49	2.64	1.80	0.0077	-
QQ1-04	713.00	2.64	1.30	0.0085	-
QQ1-05	715.15	2.62	1.80	0.0213	-
QQ1-06	717.80	2.62	0.90	0.0056	-
QQ1-07	719.50	2.63	2.00	0.4699	-
QQ1-08	721.50	2.64	1.00	0.1263	-
QQ1-09	712.70	2.61	2.80	0.0089	-
QQ1-10	725.00	2.60	2.50	0.0058	-
QQ1-11	727.12	2.63	0.90	0.0079	-
QQ1-12	729.92	2.60	1.80	0.0091	-
QQ1-13	732.75	2.59	1.90	0.0076	-
QQ1-14	735.36	2.62	1.30	0.0168	-
QQ1-15	738.50	2.60	2.20	0.0076	-
QQ1-16	740.60	2.61	1.70	0.0074	-
QQ1-17	741.50	2.64	1.50	0.0993	-
QQ1-18	744.10	2.64	1.00	0.0322	-
QQ1-19	747.10	2.63	1.20	0.0104	-
QQ1-20	749.50	2.59	1.80	0.0087	-
QQ1-21	750.50	2.60	1.40	0.1754	-
QQ1-22	752.57	2.63	0.80	0.0093	-
QQ1-23	754.63	2.63	1.70	0.0240	-
QQ1-24	756.70	2.62	0.90	0.0105	-
QQ1-25	758.77	2.62	1.20	0.3384	-
QQ1-26	760.83	2.61	1.20	0.0103	-
QQ1-27	762.90	2.64	1.10	0.0106	-
QQ1-28	764.97	2.62	1.10	0.0192	-
QQ1-29	767.03	2.61	2.00	0.0881	-
QQ1-30	769.10	2.60	1.50	0.0088	-
QQ1-31	771.17	2.59	1.40	0.0096	-
QQ1-32	773.23	2.61	0.90	0.0082	-
QQ1-33	775.30	2.60	0.90	0.0081	-
QQ1-34	777.37	2.59	0.60	0.0089	-
QQ1-35	779.43	2.58	1.30	0.0061	-
QQ1-36	781.50	2.56	1.30	0.0185	-
QQ1-37	785.50	2.52	1.80	0.0064	-
QQ1-38	783.30	2.53	1.80	0.0129	-
QQ1-39	787.50	2.48	1.10	0.0265	-
QQ1-40	789.60	2.42	2.10	0.0055	-
QQ1-41	791.60	2.43	3.40	0.0792	-
QQ1-42	793.60	2.54	0.70	0.0046	-
QQ1-43	795.60	2.65	1.20	0.0092	-

Note that en dash indicates that the measurement is not available.

in the Longmaxi Formation shale, the pore connectivity of which was much higher than other pore types (**Figures 4I–L**).

The densities of the Longmaxi Formation shale generally vary from 2.42 to 2.69 g/cm^3 (average, 2.61 g/cm^3) (**Table 4**). The porosity of the Longmaxi Formation shale mainly ranges from 1 to 2% (average, 1.51%) (**Table 4** and **Figure 5A**), and permeability ranges from 0.001 to 0.05 $\times$ 10^{-3} μm^2 (average, 0.035 $\times$ 10^{-3} μm^2) (**Table 4** and **Figure 5B**). The specific surface of the Longmaxi Formation shale ranges from 1.22 to 5.17 m^2/g (**Table 4**).

DISCUSSION

Diagenetic Evolution History

Diagenetic evolution was closely related to sedimentary processes and structural evolution, because rapid deposition can accelerate diagenetic evolution, whereas a structural uplift can weaken or even stop diagenetic evolution (Curtis, 1978; Dong et al., 2015). The Sichuan Basin is a polyhistory basin, which experienced multi-stage tectonic movements (Liu et al., 2011). The diagenetic products and geochemistry can reconstruct the diagenetic evolution history of the Longmaxi Formation (**Figure 6**), in which structural history, burial history, thermal history, and Ro evolution were based on previous research (Xu et al., 2015; Liu et al., 2020).

According to the diagenetic division regime of Morad et al. (2000), diagenetic events can be divided into three regimes: eodiagenesis (0–2 km depth and <70°C), mesodiagenesis (>2 km depth and >70°C), and teleodiagenesis (uplift to near-surface exposure and weathering).

The Longmaxi Formation shale has undergone a rapid subsidence period, a rapid uplift period, and a stabile period during burial processes, which have resulted in a complicated diagenetic evolution in different burial stages (Liu et al., 2011; Wang et al., 2017b; **Figure 6**). Besides, the Longmaxi Formation shale experienced different burial and structural history in the basin margin and center (**Figure 6**). Therefore, the eodiagenesis was subdivided into two evolution stages and the mesodiagenesis (burial diagenesis) was subdivided into three evolution stages, respectively, in the basin margin and center (**Table 1** and **Figure 6**).

Diagenetic Evolution History in the Sichuan Basin Margin

Stage A of the eodiagenesis

During stage A of the eodiagenesis, the overlying Silurian system was widely deposited in the Sichuan Basin, such that the Longmaxi Formation shale was rapidly deposited and buried. The paleo-geotemperature was <60°C and the Ro values, which were calculated in a previous research of Xu et al. (2015), was <0.35% during this stage (**Figure 6**). Shale with immature organic matter was quickly isolated from surface water and gradually evolved into the eodiagenesis stage. The shale became tight with authigenic siderite and orientated minerals due to strong mechanical compaction and dehydration. Clay minerals were dominated by smectite. The pore space mainly consisted of primary pores (**Figure 3E**). The organic matter was immature, but it started to form some biogenic gas during this stage (Peters and Cassa, 1994).

Stage B of the eodiagenesis

During stage B of the eodiagenesis, the Longmaxi Formation rapidly subsided from 1,500 to 2,200 m and then slowly uplifted from 2,200 to 2,000 m (**Figure 6**). The paleo-geotemperature increased from 60 to 70°C, and the Ro reached up to 0.5% (Xu et al., 2015; **Figure 6**). The organic matter was still immature, although some more biogenic gas was formed during this stage (Peters and Cassa, 1994). The organic acids were formed by the thermal evolution before the extensive generation of hydrocarbon, so many secondary pores were formed as the result of strong acidic dissolution. Shale changed from semi-consolidated into a consolidated state due to strong mechanical compaction (**Figure 6**). Smectite gradually transformed into an illite–smectite mixed layer that was dominated by smectite (**Figure 6**). Sheet-like authigenic kaolinite was pervasive (**Figure 3F**), and authigenic quartz began to occur (**Figures 3D,E**). Some authigenic quartz gradually occurred due to clay mineral transformation and dissolution (**Figures 3C–E**, **4A**, **6**).

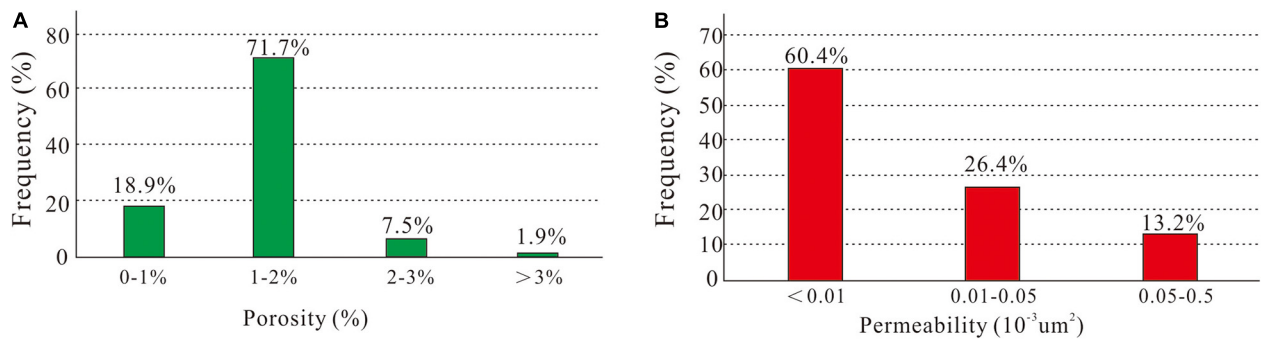

FIGURE 5 | Porosity **(A)** and permeability **(B)** histograms of the Longmaxi Formation shale in the Sichuan Basin.

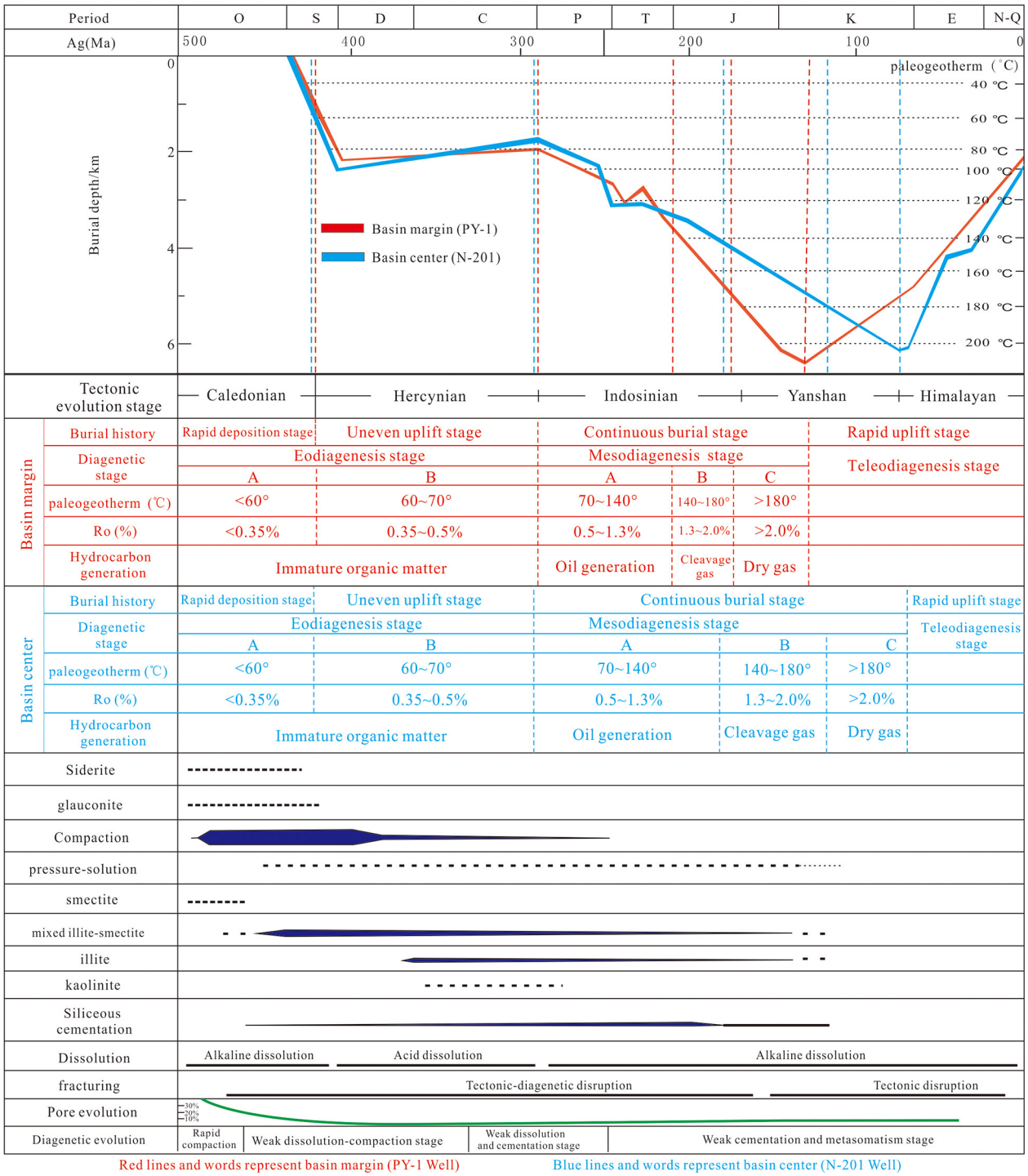

FIGURE 6 | Burial history, thermal history, and diagenetic evolution sequence of the Longmaxi Formation shale in the Sichuan Basin (the burial evolution and thermal history of well PY-1 referenced from Xu et al. (2015); the burial evolution and thermal history of well N-201 referenced from Liu et al. (2020); the diagenetic evolution sequence is modified after Wang et al. (2015)). Based on the burial history, combined with the characteristics of burial depth, temperature, thermal maturity of organic matter, authigenic mineral groups and relationships, and diagenesis, the diagenetic evolution process of different areas in Sichuan Basin is established.

Stage A of the mesodiagenesis

A large-scale relative sea level rise and marine transgression occurred from the Permian to the Early Triassic, which indicated the sustained subsidence of the Sichuan Basin (**Figure 6**) (Wang et al., 2017a). Consequently, the burial depth of the Longmaxi Formation increased from 2,000 to 4,000 m with slight fluctuation

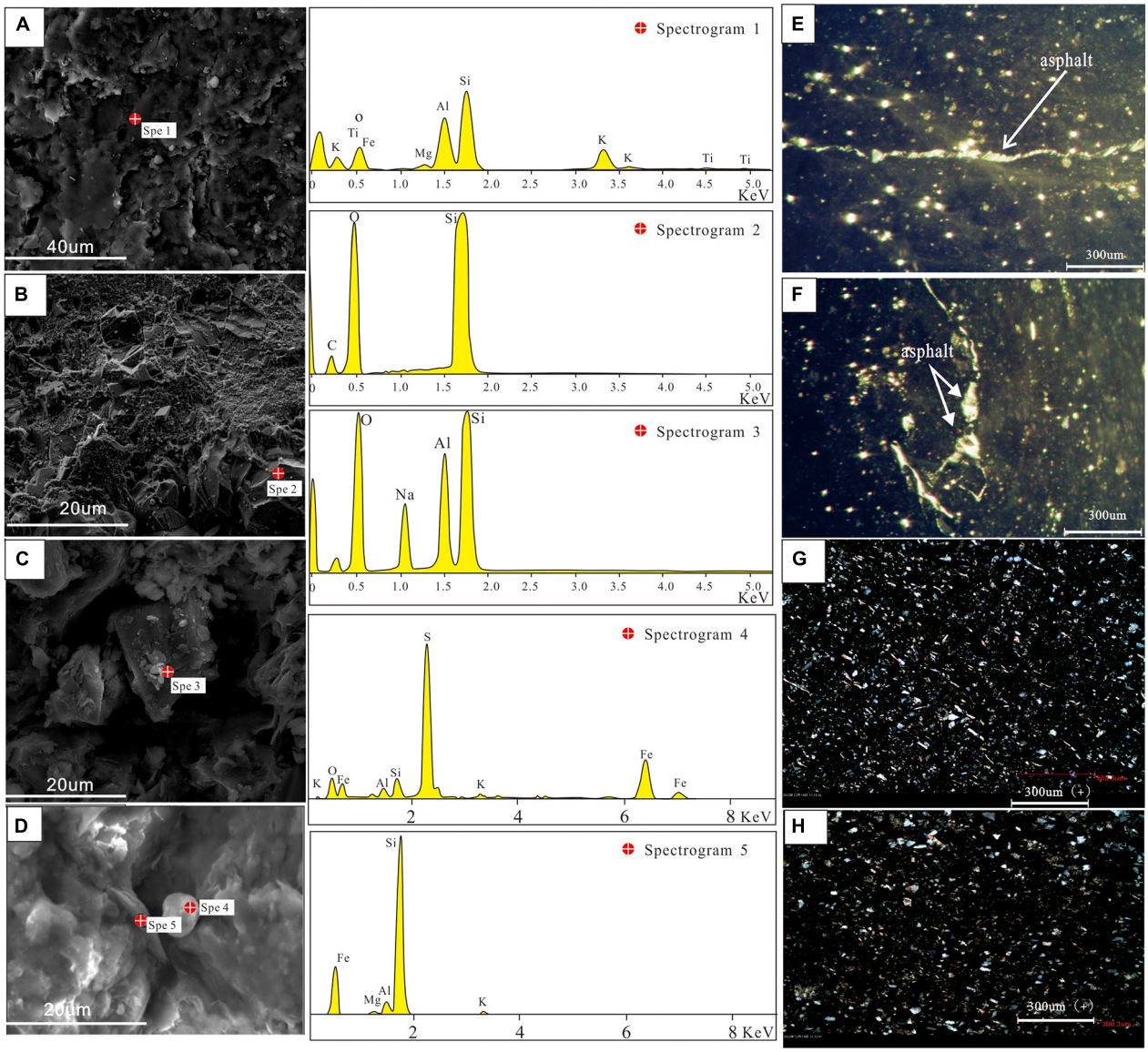

FIGURE 7 | Microscopic minerals and diagenetic characteristics of the Longmaxi Formation shale in the Sichuan Basin margin [scanning electron microscope (SEM) and energy-dispersive spectroscopy (EDS)]. **(A)** An SEM image showing the clay minerals; the right image of **(A)** is the corresponding EDS (spectrogram 1), the Shizhu section, layer 2. **(B)** An SEM image showing authigenic quartz; the right image is the corresponding EDS (spectrogram 2), the Shizhu section, layer 8. **(C)** An SEM image showing clay minerals grow on the surface of authigenic quartz; the right image is the corresponding EDS (spectrogram 3), the Shizhu section, layer 11. **(D)** An SEM image showing illite and pyrit; the right image is the corresponding EDS (spectrograms 4 and 5), the Shizhu section, layer 11. **(E)** A fluorescence microscope image showing asphalt in micro-cracks, well QQ-1, 756.13 m. **(F)** A fluorescence microscope image showing asphalt in micro-cracks, well QQ-1, 765.52 m. **(G)** Micrographs of thin sections (MTS) showing the quartz in shale, well YQ-1, 1,126.44 m. **(H)** Micrographs of thin sections (MTS) showing the quartz in shale, well YQ-1, 1,130.38 m.

during stage A of mesodiagenesis (**Figure 6**). Meanwhile, the paleo-geotemperature and Ro values, respectively, increased from 70 to 140°C and 0.5% to 1.3% (**Figure 6**). Organic matter evolved from early mature to peak mature and late mature (Peters and Cassa, 1994). Some more authigenic quartz gradually occurred due to clay mineral transformation and dissolution (**Figures 3C–E, 4A,I,J, 6**). Therefore, the Longmaxi Formation shale generated a large quantity of hydrocarbon, which was the main oil source of ancient oil reservoirs in the Sichuan Basin (Liu et al., 2011).

Phase B of the mesodiagenesis

During stage B of the mesodiagenesis, the Longmaxi Formation rapidly subsided to 5,000 m (**Figure 6**). Meanwhile, the paleo-geotemperature and the Ro, respectively, increased to 180°C and 2.0% (Xu et al., 2015; **Figure 6**). Most of organic matter transformed from late mature to postmature with the generation of pyrolysis gas (Peters and Cassa, 1994). The content of smectite in the illite–smectite mixed layer decreased obviously (**Table 3**). Clay mineral transformation accelerated the generation

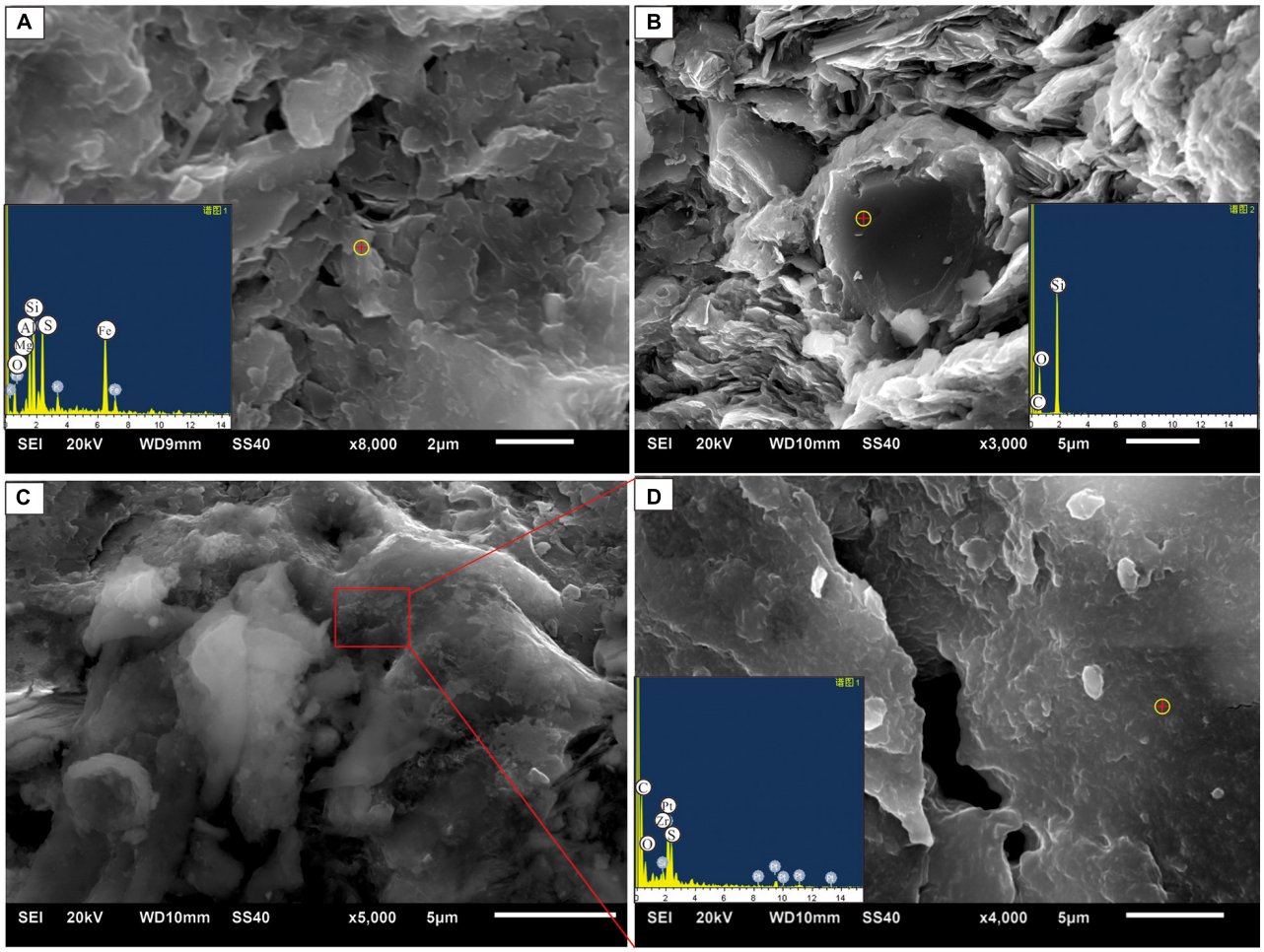

FIGURE 8 | Microscopic minerals and diagenetic characteristics of the Longmaxi Formation shale in the Sichuan Basin center (SEM and EDS). **(A)** An SEM image showing the clay minerals; the small picture in the lower left corner is the corresponding EDS, well JY-2, 2,459.36 m. **(B)** An SEM image showing authigenic quartz; the small picture in the lower right corner is the corresponding EDS, well JY-2, 2,459.36 m. **(C)** An SEM image showing asphalt organic matter in micro-cracks, well W-201, 2,678.61 m. **(D)** An SEM image that is a partial enlargement of image **(C)**; the small picture in the lower left corner is the corresponding EDS.

of authigenic quartz (**Figures 7A–D**) (Wang et al., 2017b) and authigenic grain-coating illite around detrital quartz (**Figure 7C**). The quartz was dissolved in the alkaline diagenetic environment due to depletion–expulsion of organic acids and generation–expulsion of hydrocarbon (**Figure 4F**).

Stage C of the Mesodiagenesis

The Longmaxi Formation shale was at stage C of the mesodiagenesis after the Middle Jurassic and before the Early Cretaceous. The Longmaxi Formation rapidly subsided before 130 Ma (Early Cretaceous) with a burial depth of 5,000–6,300 m and paleo-geotemperature of 180–210°C (**Figure 6**). Besides, the Ro values, which were calculated by paleo-geotemperature and burial depth in a previous research (Xu et al., 2015), were generally more than 2.0%. These indicate that the Longmaxi Formation shale was at a postmature stage of organic matter with generation of dry gas and experienced a large-scale generation-expulsion process of hydrocarbons (**Figure 6**; Wang et al., 2017a). Many microfractures were filled by a residual asphalt of organic matter evolution (**Figures 6E,F**), and a large amount of organic nanopores were formed within the organic matter (**Figures 4I–L**). The illite–smectite mixed layer nearly disappeared due to the complete transformation of clay minerals (**Table 3** and **Figure 6**).

Telediagnosis

The Sichuan Basin has gradually uplifted since the Early Cretaceous (130 Ma) because of Yanshan and Himalayan movement, which generated many large faults (**Figure 6**; Liu et al., 2011). The paleo-geotemperature subsequently decreased from 200 to 80°C due to an uplift from 6,300 to 2,000 m, which could have slowed down or stopped mesodiagenesis (Wang et al., 2017b). A relatively open-pressure system, which was caused by some large vertical faults, resulted in a massive loss of conventional oil and gas reservoirs in the Sichuan Basin (Liu et al., 2011; Wang et al., 2017a). Therefore, many secondary pores and micro-fractures were formed in the open system of uplift zone (**Figures 4E–H**).

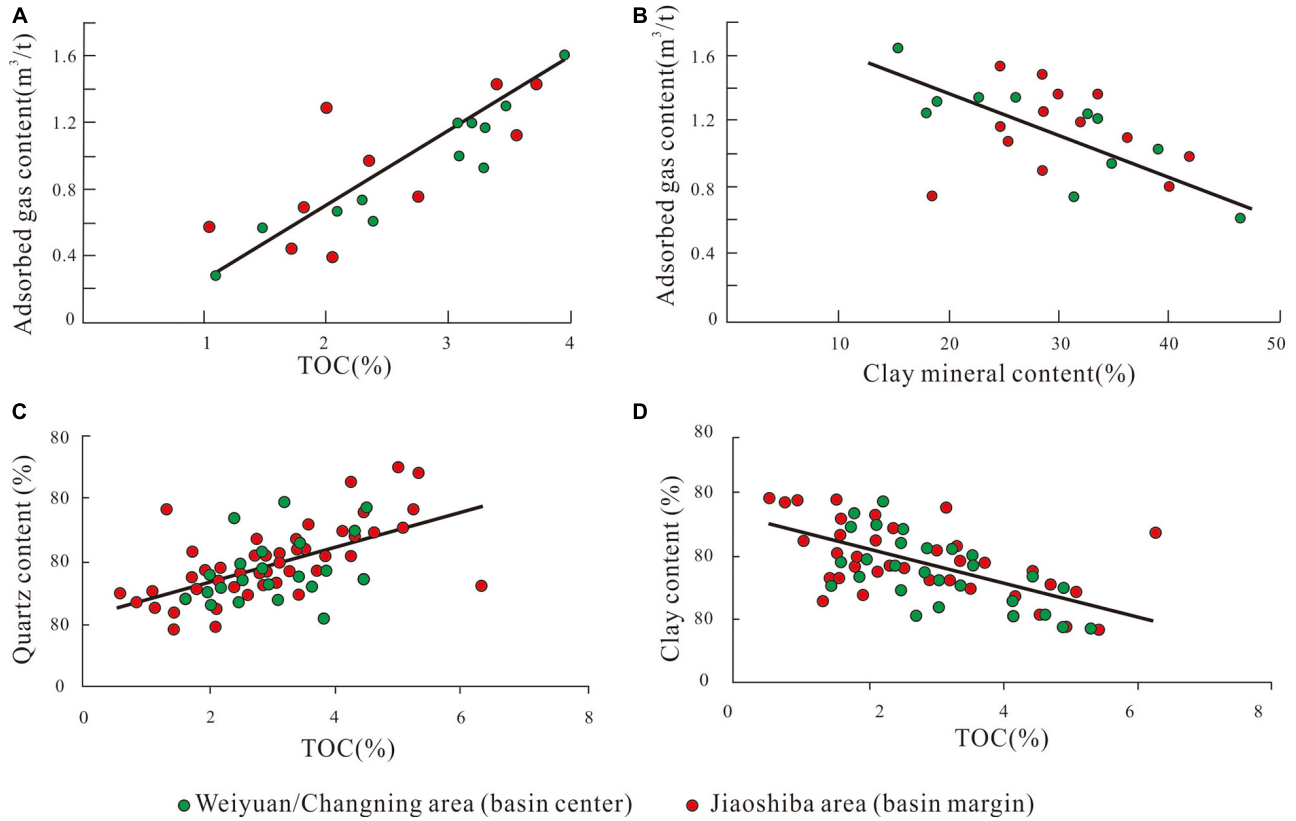

FIGURE 9 | Relationship maps between absorbed gas content and total organic carbon (TOC) and mineral content in the Sichuan Basin (the data of Jiaoshiba area was referenced from Guo et al. (2014)). **(A)** A scatter diagram of TOC and absorbed gas content. **(B)** A scatter diagram of absorbed gas and clay mineral content. **(C)** A scatter diagram of quartz content and TOC. **(D)** A scatter diagram of clay mineral content and TOC.

Diagenetic Evolution History in the Sichuan Basin Center

There are some differences in the burial evolution history between the central and marginal areas of the Sichuan Basin (**Figure 5**). According to the burial depth, paleo-temperature, Ro, and diagenesis characteristics of the Longmaxi Formation shale in well N-201 (Liu et al., 2020; **Figure 6**), combined with the diagenetic division regime of Morad et al. (2000), the diagenetic evolution of the Longmaxi Formation in the central Sichuan Basin can also be divided into six different stages (**Figure 6**).

There are no differences in the burial, thermal, and diagenetic history between the central and marginal Sichuan Basin during phase A and B of the eodiagenesis (**Figure 6**). However, the Longmaxi Formation shale in the central basin contains more carbonate minerals (average, 13.34%) and less feldspars (average, 3.35%) than the basin margin due to the early different sedimentary environment (**Table 2**).

The Longmaxi Formation continuously subsided from 300 to 80 Ma during phase A–C of the mesodiagenesis in the central basin, whose subsidence duration was longer than that in the basin margin (**Figure 6**). Besides, the average contents (23.3–33.0%) of mixed illite–smectite are obvious less than those of the basin margin (40.9–67.9%) (**Table 3**). Therefore, the compaction and clay mineral transformation of the Longmaxi Formation were stronger in the central basin than the basin margin (**Figure 8A**). The average quartz content in the central basin (50.0%) is generally higher than that in the basin margin (35.8–52.3%), indicating stronger silicification (**Table 2** and **Figure 8B**). The organic matter experienced more intense thermal evolution due to a longer subsidence duration. Besides, there are a lot of asphalt in pore space (**Figures 8C,D**). The existence of organic acids inhibits abundant quartz dissolution in the Longmaxi Formation of the central basin (Wang et al., 2017b).

The Longmaxi Formation has been uplifting since the Late Cretaceous (80 Ma) in the central basin (**Figure 6**). The relative closed diagenetic system of the central basin owing to shorter uplift duration resulted in the absence of fresh water leaching and fractures in the central basin compared to the basin margin.

Main Controlling Factors of Diagenesis

The low-energy, anoxic marine shelf environment is favorable for the sedimentation of black mud with abundant organic matter, which is the source of biogenic quartz cementation (**Figure 3C**). Clay mineral transformation and compaction were influenced by clay and brittle mineral composition of primary sediments. Besides, abundant soluble constituents of shale, which mainly derived from provenance, were material basis of dissolution (**Figures 4E,F**). The composition of shale was determined

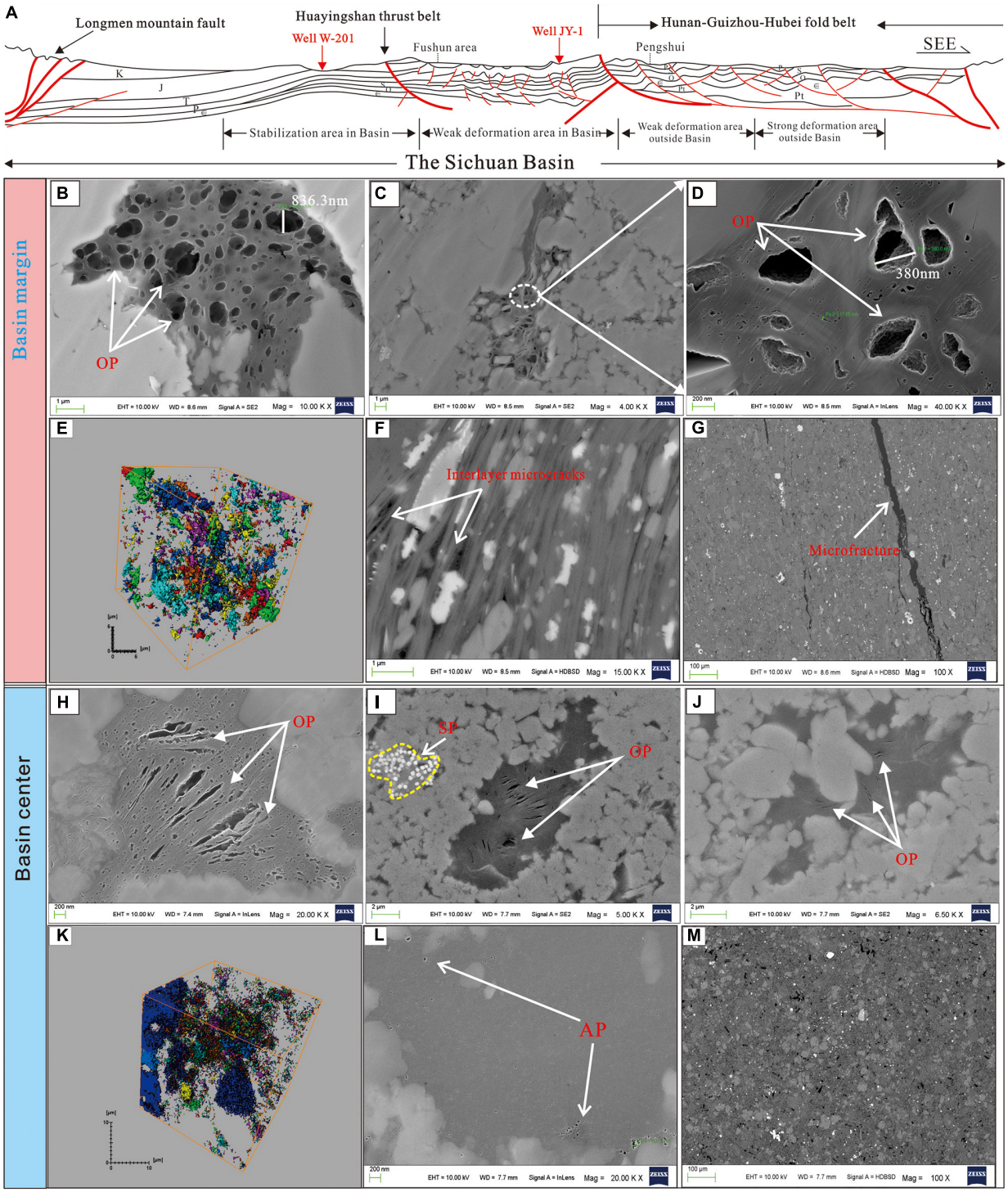

FIGURE 10 | Microscopic characteristics of reservoirs in different structural regions in the Sichuan Basin. **(A)** Different structural characteristics of the central and marginal areas in the Sichuan Basin. **(B)** An FESEM image showing the organic pores (OPs), well JY-2, 2,459.36 m. **(C)** An FESEM image showing the organic pores (OPs), well JY-2, 2,459.36 m. **(D)** An FESEM image showing the organic pores (OPs), which is a partial enlargement of image **(C)**, well JY-2, 2,459.36 m. **(E)** A field emission scanning electron microscope combined with a focused ion beam (FIB-FESEM) image showing the 3-D structure of pore spaces (different colors represent different types of pore spaces), well JY-2, 2,459.36 m. **(F)** FESEM images showing interlayer micro-cracks, well JY-2, 2,459.36 m. **(G)** FESEM images showing a micro-fracture of shale, well JY-2, 2,459.36 m. **(H)** An FESEM image showing the organic pores (OPs), well N-203, 2,325.64 m. **(I)** An FESEM image showing the organic pores (OPs) and strawberry pyrite (SP), well W-201, 2,678.61 m. **(J)** An FESEM image showing the organic pores (OPs), well W-201, 2,678.61 m. **(K)** An FIB-FESEM image showing the 3-D structure of pore spaces (different colors represent different types of pore spaces), well W-201, 2,678.61 m. **(L)** An FESEM image showing intragranular pore spaces (APs), well W-201, 2,678.61 m. **(M)** An FESEM image of the overall micro-characteristics of shale, well W-201, 2,678.61 m.

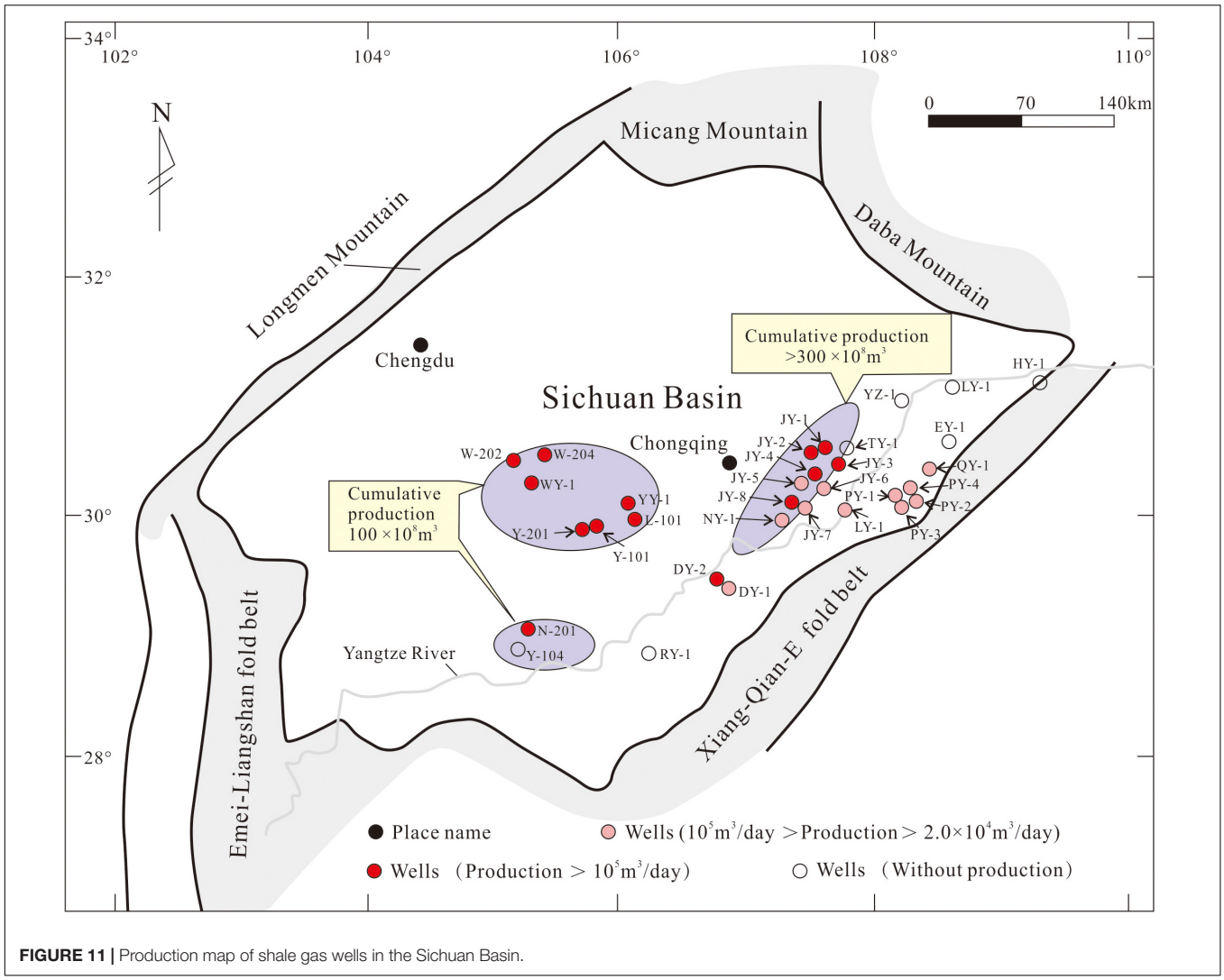

FIGURE 11 | Production map of shale gas wells in the Sichuan Basin.

by the provenance and sedimentary environment. Therefore, sedimentology characteristics is one of the most important controlling factors of diagenesis (Boles and Franks, 1979; Li and Liu, 2009).

The clay mineral transformation, compaction, and thermal evolution of organic matter were controlled by the burial depth and paleo-geotemperature during different diagenetic stages (**Figure 6**). Besides, the organic acids of dissolution were derived from the thermal evolution of organic matter. The burial depth and paleo-geotemperature were generally determined by the structural evolution (**Figure 6**). Therefore, the complex diagenetic evolution of the Longmaxi Formation shale was the result of a complicated structural history.

Influence of Diagenetic Evolution on Shale Gas Exploration and Development

Mineral Composition of Shale Reservoir

Absorbed gas, which is mainly stored within organic matter, is the most important occurrence of shale gas (Curtis, 2002). There are positive correlations between TOC and absorbed capacity of gas in the Longmaxi Formation shale of Sichuan Basin (**Figure 9A**). Besides, there is a negative correlation between clay mineral content and absorbed gas content (**Figure 9B**). In general, the TOC content of organic-rich shale increases with increasing content of clay mineral and decreasing content of quartz (Mou et al., 2011). However, there is a positive correlation between TOC and quartz content (**Figure 9C**) and an obvious negative correlation between TOC and clay minerals (**Figure 9D**). These indicate that some biogenetic silicification (**Figure 3C**; Wang S. F. et al., 2014) and clay mineral transformation added to the quartz content by forming authigenic quartz (**Figures 3D,E**, **4A**; Wang et al., 2017b). Therefore, the absorbed capacity of the Longmaxi Formation shale gas was related to mineral composition, which was influenced by the sediment characteristics and diagenetic evolution. The high contents of quartz and low content of the Longmaxi Formation suggest a strong absorbed capacity of shale both in the basin margin and center (**Table 2**).

Artificial fracturing is the most important method for shale gas development, which was influenced by the contents of

brittle minerals (Curtis, 2002; Jarvie et al., 2007). The high contents of brittle minerals both in the basin margin and center (**Table 1**), which was determined by sediment characteristics and silicification, were beneficial for artificial fracturing of shale gas development.

Reservoir Characteristics of Shale

A methane molecule is only 0.38 nm, which is comparable to a water molecule and thus easily enriched in shale (Jarvie, 2008). Organic matter volume can occupy 14% of the total shale volume when TOC content reached 7% in shale (Jarvie, 2008). Meanwhile, the shale porosity can increase by 4.9%, if 35% of the organic matter undergoes thermal evolution (Jarvie, 2008). Thus, the mass transfer of diagenetic system may be related to organic matter evolution, which resulted in the formation of secondary pores (**Figures 4D–F**) and organic pores (**Figures 4J–L**).

The organic micropores mainly occur as honeycomb-like subrounded nanopores (**Figures 10B,D**) in the Longmaxi Formation shale of the basin margin. In contrast, organic nanopores space of the Longmaxi Formation shale are generally long strip in the central basin (**Figures 10H–J**). The feldspar contents of the basin margin are obviously more than those in the central basin (**Table 2**), which provided more soluble constitute for the dissolution in the basin margin. Besides, micro-fractures of the Longmaxi Formation shale mainly developed in the basin margin (**Figures 10A,E-G**) but rarely in the central basin (**Figures 10A,L,M**). These suggest that the more open diagenetic system was in favor for the formation and preservation of secondary dissolved pores and organic pores in the basin margin and that the relatively stronger compaction resulted in the deformation of pore space in the central basin due to different burial history and diagenetic evolution (**Figures 6**, **10**).

Results of Shale Gas Development

More shale gas wells were drilled in the basin margin than the central basin (**Figure 11**). Besides, the cumulative gas production of the Longmaxi Formation shale is more than 300×10^8 m^3 in the basin margin and just 100×10^8 m^3 in the central basin (**Figure 11**). These also suggest and prove that the Longmaxi Formation shale in the basin margin with late weak tectonic reformation might have a better exploration and development potential of shale gas than the central basin.

CONCLUSION

The diagenetic evolution can be divided into three regimes: eodiagenesis, mesodiagenesis, and telediagnosis. The eodiagenesis was subdivided into two evolution stages and the mesodiagenesis was subdivided into three evolution stages, respectively, in the basin margin and center.

Provenance and sedimentary environment control the material basis of diagenetic evolution. Structural evolution determined the diagenetic evolution by influencing burial and thermal history. The diagenetic system in the basin margin was more open than that in the basin center due to a different structural and burial history.

The absorbed capacity and artificial fracturing effect of the Longmaxi Formation shale gas were related to mineral composition, which was influenced by the sediment characteristics and diagenetic evolution. The high contents of quartz (brittle minerals) and low clay mineral content of the Longmaxi Formation suggest a strong absorbed capacity and good artificial fracturing of shale both in the basin margin and center.

The mass transfer of diagenetic system may be related to organic matter evolution, which resulted in the formation of secondary pores and organic pores. The more open diagenetic system consisting of more micro-fractures and soluble constitute (e.g., feldspar) was in favor for the formation and preservation of secondary dissolved pores and organic pores in the basin margin. The relatively closed diagenetic system with stronger compaction resulted in the deformation of pore space in the central basin due to a different burial history and diagenetic evolution.

DATA AVAILABILITY STATEMENT

The original contributions presented in the study are included in the article/supplementary material, further inquiries can be directed to the corresponding author/s.

AUTHOR CONTRIBUTIONS

JW contributed as the major author of the manuscript. XT and JT did a part of writing and coding works. LL, XG, CL, and CZ provided some interesting ideas. LZ provided the suggestions. LZ and WX gave analysis on results. CL and WX collected the data. All authors contributed to the article and approved the submitted version.

FUNDING

This work was financially supported by the National Natural Science Foundation of China (Grant Numbers 42072140 and 41902153) and the Natural Science Foundation Project of CQ CSTC (Grant Numbers cstc2018jcyjAX0523 and cstc2020jcyj-msxm0778).

ACKNOWLEDGMENTS

We greatly thank the Exploration and Development Research Institute of Southwest Oil and Gas Field Company and Chongqing Institute of Geology and Mineral Resources for providing all the related core samples, geological data, and permission to publish these data. We thank our scientific research team for their help and guidance in the field investigation.

REFERENCES

Allen, P. A., and Allen, J. R. (1990). *Basin Analysis: Principles and Applications to Petroleum Play Assessment*. Oxford: Wiley-Blackwell, 263–308.

Archer, S. G., Wycherley, H. L., Watt, G. R., and Chen, H. (2004). Evidence for focused hot fluid flow within the Britannia Field, offshore Scotland, UK. *Basin Res.* 16, 377–395. doi: 10.1111/j.1365-2117.2004.00240.x

Bjørlykke, K. (1993). Fluid flow in sedimentary basins. *Sediment. Geol.* 86, 137–158. doi: 10.1016/0037-0738(93)90137-t

Bjørlykke, K. (2014). Relationship between depositional environments, burial history and rock properties. Some principal aspects of diagenetic process in sedimentary basins. *Sediment. Geol.* 301, 1–14. doi: 10.1016/j.sedgeo.2013.12.002

Bjørlykke, K., and Jahren, J. (2012). Open or closed geochemical systems during diagenesis in sedimentary basins: Constraints on mass transfer during diagenesis and the prediction of porosity in sandstone and carbonate reservoirs. *AAPG Bull.* 96, 2193–2214. doi: 10.1306/04301211139

Boles, J. R., and Franks, S. G. (1979). Clay diagenesis in wilcox sandstones of southwest texas–implications of smectite-illite reaction for sandstone cementation: abstract. *J. Sediment. Petrol.* 49, 55–70.

Buhman, C. (1992). Smectite-to-Illite conversion in a geothermally and lithologically complex Permian sedimentary sequence. *Clay Clay Miner.* 40, 53–64. doi: 10.1346/ccmn.1992.0400107

Burtner, R. L., and Warner, M. A. (1986). Relationship between illite/smectite diagenesis and hydrocarbon generation in Lower Cretaceous Mowry and Skull Creek shales of Northern Rocky Muntain Area. *Clay Clay Miner.* 34, 390–402. doi: 10.1346/ccmn.1986.0340406

Curtis, C. D. (1978). Possible links between sandstone diagenesis and depth-related geochemical reactions occurring in enclosing mudstones. *J. Geol. Soc. Lond.* 135, 107–114. doi: 10.1144/gsjgs.135.1.0107

Curtis, J. B. (2002). Fractured shale-gas systems. *AAPG Bull.* 86, 1921–1938.

Day-Stirrat, R. J., Milliken, K. L., Dutton, S. P., Loucks, R. G., Hillier, S., Aplin, A. C., et al. (2010). Open-system chemical behavior in deep Wilcox Group mudstones, Texas Gulf Coast, USA. *Mar. Pet. Geol.* 27, 1804–1818. doi: 10.1016/j.marpetgeo.2010.08.006

Dickinson, W. R. (1993). Basin geodynamics. *Basin Res.* 5, 195–196. doi: 10.1111/j.1365-2117.1993.tb00066.x

Dickinson, W., Anderson, R. N., and Biddle, K. T. (1997). *The Dynamics of Sedimentary Basins. USGC*. Washington, DC: The National Academies Press, 43.

Dong, C. M., Ma, C. F., Luan, G. Q., Lin, C. Y., Zhang, X. G., and Ren, L. H. (2015). Pyrolysis simulation experiment and diagenesis evolution pattern of shale. *Acta Sedimentol. Sin.* 33, 1053–1061. (in Chinese),

Guo, X. S., Hu, D. F., Wen, Z. D., and Liu, R. B. (2014). Major factors controlling the accumulation and high productivity in marine shale gas in the Lower Paleozoic of Sichuan Basin and its periphery: a case study of the Wufeng-Longmaxi Formation of Jiaoshiba area. *Geol. China* 41, 893–901. (in Chinese),

He, D. F., Zhao, W. Z., Lei, Z. Y., Qu, H., and Chi, Y. L. (2000). Characteristics of composite petroleum systems of superimposed basins in China. *Earth Sci. Front.* 7, 23–37. (in Chinese),

Jacob, H. (1985). Disperse solid bitumens as an indicator for migration and maturity in prospecting for oil and gas. *Erdöl Und Kohle-Erdgas-Petrochemie* 38, 364–366.

Jarvie, D. M. (2008). *Unconventional Shale Resource Plays: Shale Gas Shale Oil Opportunities. Fort Worth Buiness Press Meeting*. Texas, TX: Fort Worthenss Press, 7–17.

Jarvie, D. M., Hill, R. J., Ruble, T. E., and Pollastro, R. M. (2007). Unconventional shale-gas systems: the Mississippian Barnett Shale of north-central Texas as one model for thermogenic shale-gas assessment. *AAPG Bull* 91, 475–499. doi: 10.1306/12190606068

Jia, D., Qiu, Y., Li, C., and Cai, Y. (2019). Propagation of pressure drop in coalbed methane reservoir during drainage stage. *Adv. Geo Energy Res.* 3, 387–395. doi: 10.26804/ager.2019.04.06

Kong, L. M., Wan, M. X., Yan, Y. X., Zou, C. M., Liu, W. P., Tian, C., et al. (2015). Reservior diagenesis research of Silurian Longmaxi Formation in Sichuan Basin. *Nat. Gas Geosci.* 26, 1547–1555. (in Chinese),

Lai, J., Wang, G., Cao, J., Xiao, C., Wang, S., Pang, X., et al. (2018). Investigation of pore structure and petrophysical property in tight sandstones. *Mar. Pet. Geol* 91, 179–189. doi: 10.1016/j.marpetgeo.2017.12.024

Lai, J., Wang, G., Chai, Y., Xin, Y., Wu, Q., Zhang, X., et al. (2017). Deep burial diagenesis and reservoir quality evolution of high-temperature, high-pressure sandstones: examples from Lower Cretaceous Bashijiqike Formation in Keshen area, Kuqa depression, Tarim basin of China. *AAPG Bull.* 101, 829–862. doi: 10.1306/08231614008

Lai, J., Wang, G., Ran, Y., and Zhou, Z. (2015). Predictive distribution of high quality reservoirs of tight gas sandstones by linking diagenesis to depositional facies: evidences from Xu-2 sandstones in Penglai area of central Sichuan Basin, China. *J. Nat. Gas Sci. Eng.* 23, 97–111. doi: 10.1016/j.jngse.2015.01.026

Lai, J., Wang, G., Ran, Y., Zhou, Z., and Cui, Y. (2016). Impact of diagenesis on the reservoir quality of tight oil sandstones: the case of Upper TriassicYanchang Formation Chang 7 oil layers in Ordos Basin, China. *J. Petrol. Sci. Eng.* 145, 54–65. doi: 10.1016/j.petrol.2016.03.009

Law, B. E., and Curtis, J. B. (2002). Introduction to unconventional petroleum systems. *AAPG Bull.* 86, 1851–1852.

Li, D. S. (2013). China's multicycle superimposed petroliferous basins: theory and explorative practices. *Xinjiang Petrol. Geol.* 34, 497–503. (in Chinese)

Li, S. T. (1995). Geodynamics of sedimentary basins—the main trend of basin research. *Earth Sci. Front.* 2, 1–8. (in Chinese)

Li, Z., and Li, H. S. (1994). An Approach to genesis and evolution of secondary porosity in deeply buried sandatone reservoirs, Dongpu Deprseeion. *Chin. J. Geol.* 29, 1267–1275. (in Chinese)

Li, Z., and Liu, J. Q. (2009). Key problems and research trend of diagenetic geodynamic mechanism and spatio-temporal aistrbution in sedimentary basins. *Acta Sedimentol. Sin.* 27, 837–847. (in Chinese)

Li, Z., Fei, W. H., Shou, J. F., and Wang, S. L. (2003). Overpressure and fluid in the Dongpu Depression, North China: their constraints on diagenesis of reservoir scndstones. *Acta Geol. China* 77, 126–134. (in Chinese)

Liang, D. G., Guo, T. L., Che, J. P., Bian, L. Z., and Zhao, J. (2008). Distribution of four suits of regional marine source rocks, South China. *Mar. Origin Petrol. Geol.* 13, 1–16. (in Chinese)

Liu, S. G., Li, Z. W., Sun, W., Deng, B., Luo, Z. L., Wang, G. Z., et al. (2011). Basic geological features of superimposed baisn and hydrocarbon accumulatuion in Sichuan Basin, China. *Chin. J. Geol.* 46, 233–257. (in Chinese)

Liu, W. P., Zhou, Z., Wu, J., Luo, C., Wu, W., Jiang, L., et al. (2020). Hydrocarbon generation and shale gas accumulation in the Wufeng?Longmaxi formations, Changning shale?gas field, Southern Sichuan Basin. *J. Nanjing Univ. Nat. Sci.* 56, 393–404. (in Chinese)

Loucks, R. G., Reed, R. M., Ruppel, S. C., and Jarvie, D. M. (2009). Morphology, genesis, and distribution of nanometer-scale pores in siliceous mudstones of the Mississippian Barnett Shale. *J. Sediment. Res.* 79, 848–861.

Luan, G. Q., Dong, C. M., Ma, C. F., Lin, C. Y., Zhang, J. Y., Lv, X. W., et al. (2016). Pyrolysis simulation experiment study on diagenesis and evolution of organic-rich shale. *Acta Sedimentol. Sin.* 34, 1208–1216. (in Chinese)

Luo, L., Gao, X., Gluyas, J., Tan, X., Cheng, C., Kong, X., et al. (2019). Reservoir quality prediction of deeply buried tight sandstones in extensively faulted region: a case from the Middle-Upper Jurassic Shishugou Group in central Junggar Basin, NW China. *J. Petrol. Sci. Eng.* 175, 22–45. doi: 10.1016/j.petrol.2018.12.027

Lv, D. W., Li, Z. X., Feng, T. T., Li, Y., Wang, D. D., Liu, H. Y., et al. (2015). The characteristics of coal bed 1 and oil shale 2 qualities in the sea areas of Huangxian Coalfield, Eastern China. *Oil Shale* 32, 204–217. doi: 10.3176/oil.2015.3.02

Lv, D. W., Li, Z. X., Wang, D. D., Li, Y., Liu, H. Y., Liu, Y., et al. (2019). Sedimentary model of coal and shale in the Paleogene Lijiaya Formation of the Huangxian Basin: insight from Petrological and Geochemical Characteristics of Coal and Shale. *Energy Fuels* 33, 10442–10456. doi: 10.1021/acs.energyfuels.9b01299

Lv, D. W., Song, Y., Shi, L. Q., Wang, Z. L., Cong, P. Z., and Loon, A. J. V. (2020). The complex transgression and regression history of the northern margin of the Palaeogene Tarim Sea (NW China), and implications for potential hydrocarbon occurrences. *Mar. Petrol. Geol.* 112:104041. doi: 10.1016/j.marpetgeo.2019.104041

Meng, Y. L., Wei, W., Wang, W. A., Jie, X. L., Xiao, L. H., Gao, Y. T., et al. (2012). An optimization model of clay mineral transformation under overpressure setting. *J. Jilin Univ. Earth Sci. Ed.* 42, 145–152. (in Chinese)

Milliken, K. L., Esc, W. L., Reed, R. M., and Zhang, T. W. (2012). Grain assemblages and strong diagenetic overprinting in siliceous mudrocks, Barnett Shale (Mississippian), Fort Worth Basin, Texas. *AAPG Bull.* 96, 1553–1578. doi: 10.1306/12011111129

Morad, S., Ketzer, J. M., and Deros, L. F. (2000). Spatial and temporal distribution of diagenetic alterations in siliciclasticrocks: implications for mass transfer in sedimentary basins. *Sedimentology* 47, 95–120. doi: 10.1046/j.1365-3091.2000.00007.x

Mou, C. L., Zhou, K. K., Liang, W., and Guo, X. Y. (2011). Early paleozoic sedimentary environment of hydrocarbon source rocks in the middle-upper yangtze region and petroleum and gas exploration. *Acta Geol. Sin.* 85, 526–532. (in Chinese)

Peters, K. E., and Cassa, M. R. (1994). Applied source rock geochemistry. *AAPG Bull.* 60, 93–120. doi: 10.1306/m60585c5

Robert, L. L., Robert, M. R., Stephen, R., and Daniel, M. J. (2009). Morphology, genesis, and distribution of nanometer-scale pores in siliceous mudstones of the Mississippian Barnett shale. *J. Sediment. Res.* 79, 848–861. doi: 10.2110/jsr.2009.092

Schmoker, J. M. (1993). Use of formation-density logs to determine organic-carbon content in Devonian shales of the western Appalachian Basin and an additional example based on the Bakken Formation of the Williston Basin. *US Geol. Survey Bull.* 19, 1–14.

Schoenherr, J., Littke, R., Urai, J. L., Kukla, P. A., and Rawahi, Z. (2007). Polyphase thermal evolution in the Infra-Cambrian Are Group (South Oman Salt Basin) as deduced by maturity of solid reservoir bitumen. *Org. Geochem.* 38, 1293–1318. doi: 10.1016/j.orggeochem.2007.03.010

Seiver, R. (1979). Plate tectonic controls on diagenesis. *J. Geol.* 82, 127–155. doi: 10.1086/628405

Surdam, R. C. (1989). Organic-inorganic interactions and sandstone diagenesis. *Am. Assoc. Petrol. Geol. Bull.* 73, 1–23. doi: 10.1002/9781444304459.ch

Surdam, R. C., Boese, S. W., and Crossey, L. J. (1984). The chemistry of secondary porosity. *AAPG Mem.* 37, 183–200.

Wang, J., Huang, W. M., and Li, X. G. (2014). The shale Gas exploration prospect assess of the Niutitang Formation in Western Hubei and Hunan-Eastern Chongqing. *Geol. Sci. Technol. Inform.* 33, 98–103. (in Chinese)

Wang, J., Liu, S. G., Huang, W. M., Zhang, C. J., and Zeng, X. L. (2011). Oil and gas exploration prospects of Cambrian in Southern Sichuan Basin. *Geol. Sci. Technol. Inform.* 30, 74–82. (in Chinese)

Wang, J., Tan, X. F., Tian, J. C., Luo, C., Ran, B., Chen, Q., et al. (2017a). Constraints of hydrocarbon migration in Longmaxi shale in Sichuan Basin on shale gas accumulation. *Petrol. Geol. Exp.* 39, 755–762. (in Chinese with English abstract)

Wang, J., Tan, X. F., Zeng, C. L., Chen, Q., Ran, T., Xue, W. W., et al. (2017b). Process of diagenetic system in shale and its restrict on occurrence of SiO_2: a case study of the Longmaxi Formation in the southeast district of Chongqing. *Adv. Earth Sci.* 32, 292–306. (in Chinese),

Wang, R. Y., Hu, Z. Q., Dong, L., Gao, B., Sun, C. X., Yang, T., et al. (2020a). Advancemnet and trends of shale reservoir charactization and evaluation. *Oil Gas Geol.* 42, 54–65. (in Chinese),

Wang, R. Y., Hu, Z. Q., Long, S. X., Zhao, J. H., Dong, L., Du, W., et al. (2019). Differential characteristics of the Upper Ordovician-Lower Silurian Wufeng-Longmaxi shale reservoir and its implications for exploration and development of shale gas in/around the Sichuan Basin. *Acta Geol. Sin. (English Edition)* 93, 520–535. doi: 10.1111/1755-6724.13875

Wang, R. Y., Hu, Z. Q., Sun, C. X., Liu, Z. B., Zhang, C. C., Gao, B., et al. (2018). Comparative analysis of shale reservoir characteristics in the Wufeng-Longmaxi (O3w-S1l) and Niutitang (ε_1n) Formations: a case study of the Wells JY1 and TX1 in southeastern Sichuan Basin and its periphery, SW China. *Interpretation* 6, 31–45.

Wang, R. Y., Nie, H. K., Hu, Z. Q., Liu, G. X., Xi, B. B., and Liu, W. X. (2020b). Controlling effect of pressure evolution on shale reservoirs: a case study of the Wufeng-Longmaxi Formation in the Sichuan Basin. *Nat. Gas Ind.* 40, 1–11. (in Chinese)

Wang, S. F., Zo, C. N., Dong, D. Z., Wang, Y. M., Huang, J. L., and Guo, Z. J. (2014). Biogenic silica of organic-rich shale in Sichuan Basin and Its significance for shale gas. *Acta Scientianrum Nat. Universitatis Pekinensis* 50, 476–486. (in Chinese)

Wang, X. P., Mou, C. L., Wang, Q. Y., Ge, X. Y., Chen, X. W., Zhou, K. K., et al. (2015). Diagenesis of black shale in Longmaxi Formation, southern Sichuan Basin and its periphery. *Acta Petrol. Sin.* 36, 1035–1047. (in Chinese)

Wang, X., Yin, H., Zhao, X., Li, B., and Yang, Y. (2019). Microscopic remaining oil distribution and quantitative analysis of polymer flooding based on CT scanning. *Adv. Geo Energy Res.* 3, 448–456. doi: 10.26804/ager.2019.04.10

Wu, Q. M. (2018). *Shale Gas Geological Characteristics of the Lower Silurian Longmaxi formation in Weiyuan area, South Sichuan.* Master's thesis. Chengdu: Southwest Petroleum University. 31–35. (in Chinese).

Xu, E. S., Li, Z. M., and Yang, Z. H. (2015). Thermal and hydrocarbon generation history of Wufeng and Longmaxi shales in Pengshui area, eastern Sichuan Basin: a well PY1 case study. *Exp. Petrol. Geol.* 37, 494–499. (in Chinese)

Yuan, G. H., Cao, Y. C., Zan, N. M., Schula, H. M., Gluyas, J., Hao, F., et al. (2019). Coupled mineral alteration and oil degradation in thermal oil-water-feilspar systems and implications for organic-inorganic interactions in hydrocarbon reservoirs. *Geochim. Cosmochim. Acta* 248, 61–87. doi: 10.1016/j.gca.2019.01.001

Yuan, G. H., Cao, Y. C., Zhang, Y., and Gluya, J. (2017). Diagenesis and reservoir quality of sandstones with ancient "deep" incursion of meteoric freshwater –An example in the Nanpu Sag, Bohai Bay Basin, East China. *Mar. Petrol. Geol.* 82, 444–464. doi: 10.1016/j.marpetgeo.2017.02.027

Yuan, G. H., Gluya, J., Cao, Y. C., Oxtoby, H. N., Jia, Z. Z., and Wang, Y. Z. (2015). Diagenesis and reservoir quality evolution of the Eocene sandstones in the northern Dongying Sag, Bohai Bay Basin, East China. *Mar. Petrol. Geol.* 22, 77–89. doi: 10.1016/j.marpetgeo.2015.01.006

Zhang, J. C., Xu, B., Nie, H. K., Wang, Z. Y., and Lin, T. (2008). The issue of intellectual property protection in contracts management by oil and gas enterprises. *Nat. Gas Ind.* 28, 136–140. (in Chinese)

Zhao, D. F., Guo, Y. H., Yang, Y. J., Wang, S. Y., Mao, X. X., and Li, M. (2016). Shale reservoir diagenesis and its impacts on pores of the Lower Silurian Longmaxi Formation in southeastern Chongqing. *J. Palaeogeogr.* 18, 843–856. (in Chinese),

Zhao, W. Z., Zhang, G. Y., Wang, H. J., Wang, S. J., and Wang, Z. C. (2003). Basic features of petroleum geology in the superimposed petroliferous basins of China and their research methodologies. *Petrol. Explor. Dev.* 30, 1–7. (in Chinese) doi: 10.1007/s12182-015-0014-0

Zou, C. N., Yang, Z., Pan, S. Q., Chen, Y. Y., Lin, S. H., Huang, J. L., et al. (2016). Shale gas formation and occurrence in China: an overview of the current status and future potential. *Acta Geol. Sin. Engl. Ed.* 90, 1249–1283. doi: 10.1111/1755-6724.12769

Conflict of Interest: CL was employed by the company PetroChina.

The remaining authors declare that the research was conducted in the absence of any commercial or financial relationships that could be construed as a potential conflict of interest.